# Asynchronous haltere input impairs wing and gaze control in *Drosophila*

**Running title: Asynchronous haltere input**

Michael J Rauscher (mjr67@case.edu) and Jessica L Fox (jlf88@case.edu)

Case Western Reserve University Dept. Biology

**Keywords:**

Animal Behavior, Drosophila, Haltere, Insect Flight, Saccade, Multisensory Integration

## Summary Statement

Flies have balance organs called halteres that flap at the same frequency as the wings. Disrupting the haltere-wing phase relationship impairs the fly's ability to steer its head and wings.


## Abstract

Halteres are multifunctional mechanosensory organs unique to the true flies (Diptera). A set of reduced hindwings, the halteres beat at the same frequency as the lift-generating forewings and sense inertial forces via mechanosensory campaniform sensilla. Though it is well-established that haltere ablation makes stable flight impossible, the specific role of wing-synchronous input has not been established. Using small iron filings attached to the halteres of tethered flies and an alternating electromagnetic field, we experimentally decoupled the wings and halteres of flying *Drosophila* and observed the resulting changes in wingbeat amplitude and head orientation. We find that providing asynchronous haltere input drives fast saccades in the wing, and that wing and gaze optomotor responses are disrupted differently by asynchronous input. Our findings help to synthesize our understanding of the behavioral deficits that accompany haltere ablation with the known physiology of both haltere neurons and wing and neck muscles.


## Introduction

Animal locomotion, from crawling (Heckscher et al., 2015) to swimming (Wiggin et al., 2014) to walking (Wannier et al., 2001) to flight (Dickinson and Muijres, 2016), typically requires the coordinated motion of multiple body segments or appendages. Though this coordination can stem from the activity of a central pattern generator, sensory input from

proprioceptors adjusts body motions to adapt each step (Hiebert and Pearson, 1999; Noah et al., 2004). The specific timing of muscles actuating multiple appendages can significantly change the gait of a rhythmically moving animal, and thus the mechanisms ensuring limb coordination are essential to structuring adaptive locomotion. In flying flies, proprioceptors on the wing (Dickinson, 1990) and haltere (Pringle, 1948) provide crucial feedback for the control of each wingstroke, allowing flies to actively control each wingstroke to counteract their inherent pitch instability (Sun et al., 2007).

Halteres are small club-shaped organs which have evolved from the hindwings of the true flies (Diptera). Long known to be required for stable flight (Derham, 1714), the halteres do not generate significant lift, but instead primarily detect inertial forces using campaniform sensilla at their base (Agrawal et al., 2017; Gnatzy et al., 1987; Pringle, 1948). Campaniform sensilla are a key class of insect proprioceptor, sensitive to strain forces acting on and within the cuticle (Chapman and Smith, 1963; Zill and Moran, 1981). In the haltere system, afferent neurons from campaniform sensilla entrain their firing to a preferred phase of the haltere stroke cycle (Fox and Daniel, 2008; Yarger and Fox, 2018), which in *Drosophila* and most other fly taxa is biomechanically linked to the wing stroke cycle with an antiphase synchrony (Deora et al., 2015; Hall et al., 2015).

Continuous, stroke-synchronous feedback from the halteres is functionally important for wing-steering motoneurons and muscles (Dickerson et al., 2019; Heide, 1983; Pringle, 1948). These comprise a primary target of haltere afferents, mediating a suite of compensatory wing equilibrium reflexes. In the blowfly *Calliphora*, haltere afferents arising from field dF2 at the haltere base project directly to the motoneuron controlling the wing steering muscle wB1 (Fayyazuddin and Dickinson, 1996). Direct stimulation of the haltere nerve shows that it can

entrain the firing of the wB1 motoneuron (normally more sensitive to reafference from the wing) if stimulation occurs within a limited temporal window after the wing nerve's time of last firing (Fayyazuddin and Dickinson, 1999). In flying *Drosophila*, optogenetic manipulation of the halteres resets the firing phase of both the wB1 and wB2 muscles (Dickerson et al., 2019). Tethered flight behavioral experiments show that haltere ablation results in highly variable wing amplitudes and diminished wing optomotor responses (Bartussek and Lehmann, 2016; Dickinson, 1999; Mureli and Fox, 2015). How the wing motoneurons might respond to haltere input that is asynchronous with the wing's own movement remains an open question.

Neck motoneurons also receive input from haltere afferents (Namiki et al., 2018; Strausfeld and Seyan, 1985), and mediate a similar suite of gaze-stabilizing reflexes (Hengstenberg et al., 1986). Following bilateral haltere ablation, flies are incapable of modulating the gain of optomotor gaze responses (Mureli et al., 2017). In recent work, we found that the head's movements are driven primarily by vision and not by the halteres(Rauscher and Fox, 2021). Consistent with this behavior, the electrophysiological responses of the neck motoneurons are also driven mostly by vision. In larger flies, spiking responses to visual input are gated, but not modified, by haltere input: suprathreshold action potentials in these cells require haltere oscillation but are invariant to changes in haltere frequency (Huston and Krapp, 2009). These findings raise the possibility that stroke-synchronous haltere information may be dispensable during visually-guided behaviors, with haltere input acting solely as a gating source of excitatory drive onto neck motoneurons. Per this hypothesis, we would expect both wing-synchronous and wing-asynchronous haltere input to be capable of driving gaze optomotor behavior at similar or equivalent levels.

To examine how haltere input drives wing and gaze behaviors, we experimentally decoupled the movement of the wings and haltere. By adding a small iron mass to a haltere, we immobilized it, abolishing it as a source of stroke-synchronous information. Then, using two electromagnets, we drove the haltere at specific frequencies, moving it throughout its natural range of motion in a manner that was periodic and predictable but asynchronous with the wings. This movement allowed us to observe responses to wing-haltere phase relationships that do not naturally occur. We show that asynchronously-driven halteres increase the likelihood of saccadic steering changes in the wing motor output as well as the broadband noise levels of the wing's stroke amplitude. Movements of the head, by contrast, are not accompanied by an increase in broadband noise levels. However, the optomotor responses of both head and wings are significantly diminished by asynchronous haltere input. Our results help to illuminate the relative contribution of different descending visual pathways on multimodal gaze responses.

## Materials and Methods

*Animal care, haltere manipulations, and experimental trials*

Animals were reared from a colony of wild-caught *Drosophila melanogaster*. Adult female flies (aged 3-5 days post-eclosion) were cold-anaesthetized and attached to rigid tungsten pins using UV-curing dental cement. For magnetic stimulation experiments, a single iron filing was attached to the right haltere with UV-curing dental cement prior to tethering. Only iron filings of sufficient mass to immobilize the haltere with the magnets disengaged (filings in excess of 12μg, as determined in Rauscher and Fox, 2021) were used for experiments. For ablation experiments, one or both halteres were gently and completely removed using a pair of fine forceps.

Flies were given at least ten minutes to recover from haltere manipulation and tethering prior to usage in tethered flight behavioral experiments. Haltere stimulation periods lasted 3-4 seconds, which frequently evoked grooming of the haltere with the ipsilateral metathoracic leg. Time indices for grooming epochs were annotated manually and these video segments were excluded from analysis of head and wing kinematics. For filing-treated animals, successive presentations of different haltere stimulation conditions were preceded and followed by control epochs with the magnets disengaged lasting a minimum of 250ms (~50 wingbeats). For each animal, 1-6 video segments from the same experimental condition (from replicate stimulus presentations and intervening between grooming bouts) were drawn for subsequent analysis.

*Haltere stimulation*

To facilitate control over haltere stroke kinematics, two iron-core electromagnets were positioned anterior-dorsal and posterior-ventral to a tethered flying *Drosophila* (Fig. 1A). Each electromagnet was powered from a variable power supply (TP1803D, Tekpower, Montclair, CA, USA) switched through a power transistor (D1276A, Panasonic, Kadoma, Japan) and controlled via 5V TTL-level output from a data acquisition board (USB-6434, National Instruments, Austin TX, USA). Pulse trains consisted of 50% duty cycle square-wave signals alternating at 25, 36, 50, 72, 100, or 167Hz. Signals sent to the two magnets were 180° out of phase with one another to produce a dorsal-ventral oscillation of the filing-treated haltere at the commanded frequency. Electromagnets were hand-wound using electromagnet wire and, as previously estimated (Rauscher and Fox, 2021), the field strength of each magnet was approximately 2000μT at the distance of the fly's body from the axial tip of each iron core (2mm).

*Visual stimulation*

We used a wide-field vertical stripe pattern moving in the yaw aspect under the control of a 1Hz triangle wave, which was presented to the fly using a modular LED flight arena (Reiser and Dickinson, 2008). Stripes were one or two pixels wide and pseudo-randomly spaced such that average luminance of the wide-field panorama was 50%; i.e. the pattern consisted of an equivalent number of bright and dark pixels, where one pixel encompassed 3.75° of the circumference of the display (Fox et al., 2014). Different pattern velocities were achieved by varying the amplitude of the triangle wave whilst keeping the period constant.

*High-speed video and kinematic measurements*

Haltere and wing kinematics were recorded using two synchronized high-speed cameras (TS4 or IL5, Fastec Imagining, San Diego, CA, USA) with sagittal views of the fly from the left and right aspect. Recordings were made at 1000 or 2000fps for all treated animals and the majority of untreated animals, however some untreated animals were recorded at 750fps. In each video, the position of the haltere bulb was digitized using the DLTdv8 (Hedrick, 2008) or DeepLabCut (Mathis et al., 2018) software packages. Static points were manually labeled for each video at the position of the haltere base and anterior wing base. These were used to construct a common body-normalized coordinate framework for registering tracking data across animals, with the haltere base becoming the origin and the anterior wing base becoming coordinate (1,0). Coarse wingbeat elevation time series were extracted using a custom MATLAB script. Haltere stroke amplitude measurements were estimated by measuring the range of each angular position time series. For asynchronously-driven trials, video segments shorter than the minimum period of a single cycle of the given frequency were excluded. A third camera

recording at 100fps (Point Grey Chameleon3, FLIR, Wilsonville, OR, USA) provided a dorsal view used to measure head and wing kinematics. Head yaw with respect to the body axis and wing downstroke envelope kinematic time series were computed using a custom MATLAB program called Flyalyzer (https://github.com/michaelrauscher/flyalyzer), introduced previously in Rauscher and Fox, 2021. Shutter signals from each camera were recorded on the DAQ to facilitate alignment and synchronization of kinematic time series with one another and with the magnet control pulses and visual stimuli from the LED flight arena.

*Saccade detection and analysis*

Wing and head saccades were identified in kinematic traces from the 100fps camera using the amplitude (4° amplitude change in a single frame) and duration (10-100ms) thresholds described in Cellini et al., 2021. All detected saccades were used to calculate the saccade rate shown in Fig. 2C-E. For the saccade-triggered average (STA) responses shown in Fig. 2F-G (and Fig. S2A) as well as the stimulus-aligned cyclic average responses shown in Fig S2B-E, saccades were only included from 100fps video segments with concurrent high-speed tracking of the haltere and wingbeat on the lateral aspect cameras. Each 80ms saccade-triggered window used to produce the STA was baseline-subtracted and matched to a control window selected with a randomly drawn frame index from the same video segment. To produce the histograms shown in Fig. 3 and the heatmaps shown in Fig. S3, data were pooled from all available asynchronously-driven stimulus categories (up to and including 167Hz). Each frame from the 100fps camera was assigned a haltere position and wing instantaneous phase value at frame start by finding the single nearest-match frame recorded on the high-speed lateral aspect cameras (1000 or 2000 fps). Haltere angular velocity was computed as the numerical derivative of each haltere angular

position time series. Then, to assign a single angular velocity value to each frame from the 100fps camera, the root-mean-square value of the angular velocity time series was computed for all concurrent frames from the lateral aspect camera, with the sign (positive or negative) of the lateral aspect frame with the largest absolute value being applied to the result. A graphical summary of this process is included in Fig. S3A.

*Frequency-domain analyses*

For the estimation of broadband noise (Figure 4), the fast Fourier transform (FFT) was calculated using only the first 150 samples of applicable kinematic time series from the dorsal-view camera to provide a consistent spectral resolution of 0.67Hz. Time series were DC-leveled by fitting a least-squares regression line and then subtracting it out to remove linear trends. The area under the curve of the resultant FFT was then estimated using the trapezoid method. For magnetic stimulation trials, we excluded a 4Hz range centered on the stimulus frequency from the AUC determination. For 50Hz trials, which were at the Nyquist limit for the dorsal view camera, an interval spanning 46-50Hz was instead excluded from the area under the curve measurement. For trials at frequencies exceeding the Nyquist limit for the dorsal view camera (72Hz, 100Hz, 167Hz), the excluded range encompassed the baseband alias of the driven haltere frequency. A range spanning 23-27Hz was excluded from trials without magnetic stimulation (untreated, haltere immobilized, single or double haltere ablation).

For estimation of visual response magnitude (Figure 5), kinematic time series were DC-leveled as described above and zero-padded to 4096 samples. Magnitude estimates from resultant FFTs were then divided by the number of samples in each time series prior to zero-

padding to normalize magnitudes for trials of varying length. Only segments longer than 64 samples were used, resulting in a coarsest possible spectral resolution of 1.5Hz.

## Results

*Electromagnetic control of haltere stroke kinematics*

To establish magnetic control over the haltere, an iron filing was attached to the bulb (see Methods). With the electromagnets deactivated, this mass immobilized the haltere and prevented the fly from oscillating it. Activation of the electromagnets at 25, 36, 50, 72, 100, and 167 Hz resulted in movement of the haltere at the commanded frequency (Fig. 1B-F, Video S1). The natural oscillation of the halteres and wings produces an out-of-phase relationship and commanding the haltere's frequency allowed us to sample wingbeats with all possible phase relationships. Haltere tracking data was registered into a unified coordinate framework, normalized using the haltere-thorax and wing-thorax joints as common control points, allowing us to survey movement of the haltere both within and in excess of its naturalistic range of motion (Fig 1C). In all observed trials, the untreated haltere maintained its full stroke amplitude (Fig. 1G). At the highest frequency tested, 13 out of 14 flies were unable to maintain a haltere amplitude that was within the range of those observed naturally (Fig 1G, 22 of 27 replicate trials). Because this commanded haltere motion was significantly smaller than those observed at lower frequencies, we excluded 167 Hz trials from further analyses that compared across conditions (see Methods). All conditions (save for the immobilized haltere) achieved peak angular velocities that were indistinguishable from those observed in untreated animals (Fig 1H). Baseline wingbeat frequencies were indistinguishable from untreated controls for all treatments

(Fig. 1I), showing that our manipulations did not impair the gross functioning of the wing motor system.

*Asynchronous haltere movement increases wing saccade probability*

Haltere primary afferents form synaptic connections with head- and wing-steering motoneurons either directly (Fayyazuddin and Dickinson, 1996; Fayyazuddin and Dickinson, 1999) or via interneurons (Strausfeld and Seyan, 1985; Trimarchi and Murphey, 1997). These thoracic microcircuits mediate a suite of compensatory equilibrium reflexes stabilizing the orientation of the body and head during flight (Dickinson, 1999; Sherman and Dickinson, 2003; Sherman and Dickinson, 2004). To investigate the impact of asynchronous haltere input on these reflexes, we measured each animal's head yaw and wingstroke amplitudes (Fig. 2A, Video S2) using machine vision software developed previously in Rauscher and Fox, 2021.

We noted that treated flies showed significantly higher rates of wing saccades than the untreated control animals. Saccades in *Drosophila* and other flies are abrupt changes in heading, analogous to the rapid stabilizing eye movements of vertebrates (Cellini and Mongeau, 2020; Cellini et al., 2021; Land, 1973; Land and Collett, 1974). In tethered flight, saccades appear as sharp changes in wing amplitude (Fig. 2B, Video S2). For each condition, we calculated the saccade rate (after Cellini et al., 2021) and found that all treatments exhibited higher ipsilateral wing saccade rates than untreated controls. Active asynchronous drive of the haltere at any frequency resulted in ipsilateral wing saccade rates comparable to those seen with bilateral haltere ablation, whereas haltere immobilization resulted in intermediate saccade rates comparable to those seen with unilateral ablation (Fig 2C). A similar pattern was observed for contralateral wing saccades (Fig 2D), with all treatment groups exhibiting higher saccade rates

than untreated control animals. In contrast, the head saccade rate was insensitive to haltere manipulation under all tested conditions save for bilateral ablation (Fig 2E), in agreement with previous findings that proprioceptive mechanosensory inputs, likely in the neck, are the primary driver of head saccades (Cellini et al., 2021).

*Haltere kinematic parameters influencing saccade initiation*

In individual trials, fast Fourier transforms (FFTs) of wing and head kinematic time series (Fig S1) showed elevated spectral power at the magnetic stimulation frequency (or its baseband alias for frequencies which exceeded the Nyquist limit of the camera measuring the wingstroke amplitude). Does the increased saccade rate explain the increase in power at the stimulation frequency? Surprisingly, the average rate of ipsilateral wing saccades appeared uniform across magnetic stimulation frequencies, and that rate was indistinguishable from that seen with bilateral ablation of the haltere input. Despite this, saccade-triggered average responses of the ipsilateral wing amplitude (Fig. 2F) and instantaneous frequency (Fig. 2G) tended to recapitulate the frequency of the driving stimulus for asynchronous trials. A frequency modulation component was not evident in untreated animals, for which wing saccades were also significantly smaller in amplitude (Fig. S2A). Stimulus-triggered cyclic averages aligned on each magnetic stimulation pulse showed that saccade probability varied in time with the stimulus (Fig. S2B). Taken together, these data suggest that saccades were indeed phase-locked with the driving stimulus but were not reliably elicited upon every stroke cycle. Cyclic averages also illustrated that while the treated haltere's frequency and amplitude could be reliably commanded with the magnetic stimulation, the induced oscillation assumed a diversity of phase relationships with the

magnetic stimulus across animals and between trials (Fig. S2C-E). Thus, the specific position or phase of the haltere could not be predicted by the timing of the stimulus.

After observing phase-locked saccades, we sought to determine whether specific kinematic parameters drove saccade initiation. Using all available high-speed frames, we assessed the haltere's angular position, angular velocity, and phase relationship to the wingstroke cycle (Fig 3A) and found that our manipulations encompassed the naturalistic range of values observed for each of these variables. We then created histograms assessing the probability of saccade initiation as a function of each variable under each condition (Fig. 3B-C, Fig S3). The haltere's angular position (Fig. 3B) did not exhibit a strong relationship with saccade probability under any condition, although in the asynchronous condition a slight skew in the probability histogram was evident when the haltere was in the downstroke position (roughly 180-300°). In untreated animals, the haltere's angular velocity (Fig. 3C) bifurcated into frames predominately representing upstrokes and those predominately representing downstrokes, with negative and positive angular velocities respectively, and virtually no overlap with the angular velocity range observed in immobilized animals. Notably, in the asynchronously-driven haltere condition, saccades were more likely to be elicited when the haltere moved outside of its naturalistic angular velocity range. We did not identify an obvious relationship between the wing phase and the saccade probability under any condition (Fig. 3D). Similarly, multivariate heatmaps of the three possible combinations of these variables did not illuminate any trends over and above those observed in the univariate analyses (Fig. S3).

*Asynchronous haltere movement increases wingstroke amplitude variability*

Bilateral haltere ablation increases wingstroke amplitude variability (Dickinson, 1999; Mureli and Fox, 2015). Could the wing's amplitude stability be "rescued" with any periodic haltere input, or must this input be synchronous with the wings? Because variability in the time domain includes periodic input from the driven haltere (reflecting the saccadic steering changes discussed above), we estimated the broadband noise level in the frequency domain. This allowed us to estimate changes in the baseline amplitude variability, independent of the saccades, by measuring the area under the curve of the FFT, excluding a narrow frequency band encompassing the driven haltere frequency (see Methods, Fig. 4A-B).

Haltere immobilization increased the broadband noise in the ipsilateral wing amplitude (Fig. 4C) to a level comparable to that seen with unilateral ablation, whereas active asynchronous drive using the electromagnets increased it further to levels equivalent to those seen with bilateral ablation. Similar responses of a smaller magnitude were observed for the contralateral wing (Fig. 4D), with all unilateral manipulations being distinct from those seen with untreated animals and bilateral ablation. No haltere manipulation resulted in head yaw noise levels distinct from untreated animals, similar to our results when measuring saccade rate (Fig. 4E).

*Asynchronous haltere movement disrupts wing and head optomotor responses*

A major task of the fly thoracic nervous system is to integrate inertial sensory information from wingbeat-synchronous haltere afferents with descending information from the fly's motion vision system (Namiki et al., 2018; Namiki et al., 2022; Suver et al., 2016). Tethered flies adjust their gaze and wingstroke amplitude in response to widefield visual movement (Duistermars et al., 2007; Hengstenberg et al., 1986) acting through a motor pool shared with complementary reflexes driven by the halteres. We used these reflexes to drive wing

and head behaviors and examined how disrupting haltere input changed their dynamics. Concurrently with each class of haltere treatment, we presented flies with a vertical stripe pattern moving in the yaw direction at 90°/s (Fig. 5A-B,Video S3). Then, we estimated the response amplitude by measuring the magnitude of the FFT of each kinematic time series at the frequency of the visual stimulus, 1Hz (Fig. 5C). For the ipsilateral wing and head (Fig. 5D,F), all haltere manipulations resulted in categorically lower visual response amplitudes than those seen in untreated flies. For the contralateral wing, only the bilateral ablation was distinct from untreated animals (Fig. 5E).

Previous experiments showed that bilateral haltere ablation (as well as haltere immobilization) impairs the ability of flies to tune their head responses to widefield visual stimuli, instead locking the fly into a fixed low-amplitude response to all salient pattern velocities (Mureli et al., 2017). To assess the influence of our manipulations on optomotor tuning, we presented a subset of flies with a series of visual stimuli that moved at a range of pattern velocities spanning 30-240°/s. Untreated flies exhibited an optomotor tuning curve in response to these stimuli that peaked at 180°/s for wing responses (Fig.5G-H) and 90°/s for head responses (Fig. 5I), in agreement with previous studies (Duistermars et al., 2007; Mureli et al., 2017). Similar tuning curves were observed for flies with immobilized halteres (Fig. 5G-I) although with significantly lower response amplitudes than the untreated flies (Fig. S3). With the magnets engaged at 36Hz, optomotor tuning was abolished for both contralateral and ipsilateral wings. Visual pattern velocity was not a significant predictor of response amplitude for these flies (Fig 5G-H). In comparison, head responses showed lower gain relative to untreated controls, at levels comparable to those seen with haltere immobilization (Fig. 5I,S3C,F).

## Discussion

Coordinated motion of multiple appendages is so important that it is often very difficult to force them to move in uncoordinated ways. In flies, the biomechanics of the thorax forces the halteres and wings to oscillate in perfect antiphase with no input from the nervous system: elevating the wing of a dead fly with forceps depresses the haltere (Deora et al., 2015). We used stimuli both within and outside the bounds of natural haltere motions to demonstrate the effects of asynchronous haltere perturbations on wing and head movements in flying flies. In previous studies, haltere ablation or immobilization was demonstrated to be deleterious to wing amplitude stability (Dickinson, 1999; Mureli and Fox, 2015) and optomotor reflexes (Bartussek and Lehmann, 2016; Mureli and Fox, 2015; Mureli et al., 2017), but left unresolved how specific haltere information contributes to each of these behavioral outputs. Our data demonstrate that both ipsilateral and contralateral wing steering reflexes are critically impaired by asynchronous haltere input. The head, receiving a more diverse set of sensory inputs from both descending and ascending neurons and moving at a lower speed, experiences deleterious effects of asynchronous haltere input more moderately than the wings.

### *Asynchronous haltere input drives ipsilateral wing saccades*

Campaniform sensilla located at the haltere base are sensitive to compressive and shearing forces acting on and within the cuticle in which they are embedded (Chapman and Smith, 1963; Pringle, 1948; Zill and Moran, 1981). Such forces arise from the haltere's movement through its natural stroke plane and therefore scale proportionately with the bulb's angular velocity (Nalbach, 1993). Our data show that asynchronous haltere input increases the probability of steering saccades of the ipsilateral wing, and that these saccades are comparatively

more likely when the haltere moves at angular velocities outside of its naturalistic operating range. Previous results from experiments that rotated the entire body showed that the halteres are most sensitive to body angular velocity (Dickinson, 1999); our results extend this to show that the haltere's own angular velocity drives movements of the wings.

As hypothesized by Pringle (1948) and predicted in subsequent modeling (Mohren et al., 2019), different fields of campaniform sensilla should experience forces preferentially in-line with their receptive fields at different points within the stroke cycle. We might therefore predict that saccades are more or less likely to be initiated as a function of its angular position. Though our data suggest that saccades may be slightly more likely when the asynchronously-driven haltere was in the downstroke position, we did not observe a strong correspondence between haltere angular position and saccade initiation. This discrepancy may arise from the extreme sensitivity of haltere campaniform sensilla to slight perturbations in the haltere stroke path, making it difficult to achieve identical stimulus parameters across animals and between stimulus presentations.

Physiological recordings from larger flies corroborate this for both primary haltere afferents (Yarger and Fox, 2018) as well as a downstream neck motoneuron (Haag et al., 2010): the firing properties of both neuron types changed significantly when the haltere oscillated naturally versus when its motion was driven exogenously at a similar frequency. Additionally, we note that our experimental setup was not optimized to measure all wingstroke parameters that have been shown to be relevant to steering output. While we have measured the peak downstroke angle of the wing as our proxy for steering effort, the total force produced by each wingstroke is a complex function of not just the downstroke angle, but also the wing joint deviation angle and the spanwise rotation angle of the wing (Muijres et al., 2015). Nevertheless, our results indicate

that haltere input drives saccadic motions of the wings, and we identify a relationship between the haltere's angular velocity and saccade initiation.

*Haltere influence on the contralateral wing*

In previous work (Rauscher and Fox, 2021), we manipulated the stroke amplitude of a beating haltere without compromising the haltere-wing stroke synchrony and evoked a consistent wing-steering response to the magnetic stimulation. Here, we found the response to haltere perturbation was less stereotyped and more probabilistic, but in neither the present nor previous work did we observe a clear relationship between the instantaneous wing phase and haltere-evoked changes in wing kinematic parameters. This was surprising given the organization of the wing-steering motor system downstream of haltere primary afferents, a major component of which are tonic muscles which fire once every stroke cycle and control muscle tension by varying their firing phase within it (Balint and Dickinson, 2001; Heide and Götz, 1996; Lindsay et al., 2017; Tu and Dickinson, 1996). While it is possible that our manipulations preferentially elicited changes mediated only by phasic muscles, which are less sensitive to the wing phase, this seems unlikely given how thoroughly our experiments explored the parameter space of haltere angular position, angular velocity, and wingstroke phase. A more likely hypothesis is that the untreated opponent haltere (present in all of our manipulations) provides redundant input to contralateral wing motoneurons that can supersede an absent or malfunctioning ipsilateral haltere.

Our findings that asynchronous haltere input increases the saccade rate and stroke amplitude noise of the contralateral wing are consistent with previous findings that each wing receives information from both halteres. Flies are capable of apparently normal flight following

unilateral haltere ablation (Fraenkel, 1939). In *Calliphora*, input from a single haltere is sufficient to entrain the firing of the contralateral first basalare muscle following the ablation of the ipsilateral haltere and both wing nerves (Heide, 1983). Experiments rotating the fly's entire body showed that both amplitude and frequency components of haltere-wing reflexes are impaired following bilateral—but not unilateral—haltere ablation (Dickinson, 1999). Similar results were observed using a magnetic-suspension tethering system in which the fly initiated its own rotations: manipulating the bulb mass of a single haltere produced comparable changes in both clockwise and counterclockwise body saccades (Bender and Dickinson, 2006).

This bilateral integration implicates the contralateral haltere interneurons, or cHINs (Strausfeld and Seyan, 1985; Trimarchi and Murphey, 1997), which receive input from haltere afferents and represent the only known anatomical pathway through which haltere information crosses the body axis for both the wing and gaze motor control systems. Though anatomically conserved across fly taxa, these neurons have eluded physiological characterization to date, leaving many questions unresolved as to the sensory representations and transformations they mediate *en route* to their downstream motor targets. As we were unable to reliably elicit tethered flight following any manipulation of both halteres aside from total bilateral ablation, behavioral explorations of this circuit's function are unlikely to be successful. Further exploration of each haltere's influence on the contralateral wing will likely remain contingent on a more complete description of the organization and physiology of haltere-wing thoracic microcircuits.

*Asynchronous haltere input impairs optomotor head and wing responses differently*

As visual descending inputs concurrently target wing and gaze motoneurons (Chan et al., 1998; Namiki et al., 2018; Strausfeld and Seyan, 1985) we also examined multisensory

integration of haltere and visual inputs. We show that haltere-wing asynchrony critically impairs the wing optomotor response, with results similar to those observed with bilateral haltere ablation. While this impairment is unsurprising for wings, it is less obvious how the head might respond to asynchronous haltere input. Bilateral haltere ablation prevents flies from adjusting the gain of the optomotor response to different pattern velocities (Mureli et al., 2017). Here, we show that loss of one haltere (by immobilization) reduces the optomotor response gain but does not abolish pattern velocity tuning. In some of the neck motoneurons of *Calliphora*, spiking responses are abolished without concurrent haltere input and are restored with haltere movement at any frequency, even as low as 10 Hz (Huston and Krapp, 2009). If the halteres merely provided flight-state-dependent excitatory drive onto the neck motor system, then we might predict that asynchronous drive should produce gaze optomotor tuning curves with similar or equivalent gain to an unmanipulated animal.

Our data do not show this. Instead, we found that asynchronous drive of a single haltere resulted in head responses with lower gain. Assuming similarity between the neck motoneurons of *Drosophila* and *Calliphora*, the most straightforward interpretation of these data is in terms of the visual-haltere control loop (Chan et al., 1998; Dickerson et al., 2019). As modified hind wings, the halteres possess their own complement of steering muscles which, like those of the forewings, receive descending visual inputs. Activation of these muscles by the visual system allows the fly to modulate the sensory feedback it receives from the halteres, through an unresolved mechanism that may involve directly changing the haltere's stroke kinematics or altering the stiffness of the thorax-haltere joint. While the precise mechanism of action is unresolved, effects of the descending visual neurons on the haltere's muscles have been demonstrated in flies both large (Chan et al., 1998) and small (Dickerson et al., 2019), and this

allows the haltere's complement of equilibrium reflexes to serve as an indirect visual pathway onto wing and gaze motoneurons. As synchronous input from both halteres appears necessary for the full-amplitude gaze optomotor response, the loss of optomotor gain tuning following haltere ablation observed in Mureli et al. (2017) likely represent the loss of this indirect visual-haltere pathway.

**Acknowledgments**

We would like to thank Chenxin Bi and Brandon Chun for help with data collection and annotation, as well as Noah DeFino, Jesse Fritz and Lauren Metz for fly care. We would also like to thank Hillel Chiel, Bradley Dickerson, Jeremiah Didion, Alexandra Gurgis, Nicholas Kathman, Kristianna Lea, Mark Willis, Gabriella Wolff, and Alexandra Yarger for helpful commentary.

**Competing interests**

No competing interests declared.

**Funding**

This work was supported by United States Air Force Office of Scientific Research [FA9550-14-0398 and FA9550-16-1-0165 to JLF]; and National Science Foundation [1754412 to JLF].

**Data Availability**

All processed data is available in the associated Dryad repository. Raw video data available upon request. Kinematic time series for some untreated control animals in Figures 1-5 are included with a previously-published publicly available dataset (Rauscher and Fox, 2020).

## References Cited


**Agrawal, S., Grimaldi, D. and Fox, J. L.** (2017). Haltere morphology and campaniform sensilla arrangement across Diptera. *Arthropod Struct Dev* **46**, 215–229.

**Balint, C. N. and Dickinson, M. H.** (2001). The correlation between wing kinematics and steering muscle activity in the blowfly *Calliphora vicina*. *J Exp Biol* **204**, 4213–4226.

**Bartussek, J. and Lehmann, F.-O.** (2016). Proprioceptive feedback determines visuomotor gain in *Drosophila*. *R Soc Open Sci* **3**, 150562.

**Bender, J. A. and Dickinson, M. H.** (2006). A comparison of visual and haltere-mediated feedback in the control of body saccades in *Drosophila melanogaster*. *Journal of Experimental Biology* **209**, 4597–606.

**Cellini, B. and Mongeau, J. M.** (2020). Active vision shapes and coordinates flight motor responses in flies. *Proc Natl Acad Sci U S A* **117**, 23085–23095.

**Cellini, B., Salem, W. and Mongeau, J. M.** (2021). Mechanisms of punctuated vision in fly flight. *Current Biology* **31**, 4009-4024.e3.

**Chan, W. P., Prete, F. and Dickinson, M. H.** (1998). Visual input to the efferent control system of a fly's "gyroscope". *Science* **280**, 289–292.

**Chapman, K. M. and Smith, R. S.** (1963). A linear transfer function underlying impulse frequency modulation in a cockroach mechanoreceptor. *Nature 1963 197:4868* **197**, 699–700.

**Deora, T., Singh, A. K. and Sane, S. P.** (2015). Biomechanical basis of wing and haltere coordination in flies. *Proc Natl Acad Sci U S A* **112**, 1481–6.

**Derham, W.** (1714). *Physico-theology: or, a demonstration of the being and attributes of God, from His works of creation. Being the substance of XVI sermons preached in St. Mary Le Bow-church, London, at the honble Mr. Boyle's lectures, in the years 1711 and 1712*. W. and J. Innys, London, 1714.

**Dickerson, B. H., de Souza, A. M., Huda, A. and Dickinson, M. H.** (2019). Flies regulate wing motion via active control of a dual-function gyroscope. *Current Biology* **29**, 3517–3524.

**Dickinson, M. H.** (1990). Comparison of encoding properties of campaniform sensilla on the fly wing. *Journal of Experimental Biology* **261**, 245–261.

**Dickinson, M. H.** (1999). Haltere-mediated equilibrium reflexes of the fruit fly, *Drosophila melanogaster*. *Philosophical Transactions of the Royal Society B: Biological Sciences* **354**, 903–916.

**Dickinson, M. H. and Muijres, F. T.** (2016). The aerodynamics and control of free flight maneuvers in *Drosophila*. *Philosophical transactions of the Royal Society of London B: Biological Sciences* **371**, 20150388.

**Duistermars, B. J., Reiser, M. B., Zhu, Y. and Frye, M. A.** (2007). Dynamic properties of large-field and small-field optomotor flight responses in *Drosophila*. *J Comp Physiol A Neuroethol Sens Neural Behav Physiol* **193**, 787–799.

**Fayyazuddin, A. and Dickinson, M. H.** (1996). Haltere afferents provide direct, electrotonic input to a steering motor neuron in the blowfly, *Calliphora*. *J Neurosci* **16**, 5225–5232.

**Fayyazuddin, a and Dickinson, M. H.** (1999). Convergent mechanosensory input structures the firing phase of a steering motor neuron in the blowfly, *Calliphora*. *J Neurophysiol* **82**, 1916–1926.

**Fox, J. L. and Daniel, T. L.** (2008). A neural basis for gyroscopic force measurement in the halteres of *Holorusia*. *J Comp Physiol A Neuroethol Sens Neural Behav Physiol* **194**, 887–897.

**Fraenkel, G.** (1939). The function of the halteres of flies (Diptera). *Proceedings of the Zoological Society of London* **A109**, 69–78.

**Gnatzy, W., Grünert, U. and Bender, M.** (1987). Campaniform sensilla of *Calliphora vicina* (Insecta, Diptera). *Zoomorphology* **106**, 312–319.

**Haag, J., Wertz, A. and Borst, A.** (2010). Central gating of fly optomotor response. *Pnas* **107**, 20104–20109.

**Hall, J. M., McLoughlin, D. P., Kathman, N. D., Yarger, A. M., Mureli, S. and Fox, J. L.** (2015). Kinematic diversity suggests expanded roles for fly halteres. *Biol Lett* **11**, 20150845.

**Heckscher, E. S., Zarin, A. A., Faumont, S., Clark, M. Q., Manning, L., Fushiki, A., Schneider-Mizell, C. M., Fetter, R. D., Truman, J. W., Zwart, M. F., et al.** (2015). Even-skipped+ interneurons are core components of a sensorimotor circuit that maintains left-right symmetric muscle contraction amplitude. *Neuron* **88**, 314–329.

**Hedrick, T. L.** (2008). Software techniques for two- and three-dimensional kinematic measurements of biological and biomimetic systems. *Bioinspir Biomim* **3**, 34001.

**Heide, G.** (1983). Neural mechanisms of flight control in Diptera. In *Biona-report 2* (ed. Fischer, G.), pp. 35–52. Stuttgart, New York.

**Heide, G. and Götz, K. G.** (1996). Optomotor control of course and altitude in *Drosophila melanogaster* is correlated with distinct activities of at least three pairs of flight steering muscles. *Journal of Experimental Biology* **199**, 1711–1726.

**Hengstenberg, R., Sandeman, D. C. and Hengstenberg, B.** (1986). Compensatory head roll in the blowfly *Calliphora* during flight. *Proceedings of the Royal Society B: Biological Sciences* **227**, 455–482.

**Hiebert, G. W. and Pearson, K. G.** (1999). Contribution of sensory feedback to the generation of extensor activity during walking in the decerebrate Cat. *J Neurophysiol* **81**, 758–70.

**Huston, S. J. and Krapp, H. G.** (2009). Nonlinear integration of visual and haltere inputs in fly neck motor neurons. *Journal of Neuroscience* **29**, 13097–13105.

**Land, M. F.** (1973). Head movement of flies during visually guided flight. *Nature 1973 243:5405* **243**, 299–300.

**Land, M. F. and Collett, T. S.** (1974). Chasing behaviour of houseflies (*Fannia canicularis*). *Journal of comparative physiology 1974 89:4* **89**, 331–357.

**Lindsay, T., Sustar, A. and Dickinson, M. H.** (2017). The function and organization of the motor system controlling flight maneuvers in flies. *Current Biology* **27**, 345–358.

**Mathis, A., Mamidanna, P., Cury, K. M., Abe, T., Murthy, V. N., Mathis, M. W. and Bethge, M.** (2018). DeepLabCut: markerless pose estimation of user-defined body parts with deep learning. *Nat Neurosci* **21**, 1281–1289.

**Mohren, T. L., Daniel, T. L., Eberle, A. L., Reinhall, P. G. and Fox, J. L.** (2019). Coriolis and centrifugal forces drive haltere deformations and influence spike timing. *J R Soc Interface* **16**, 20190035.

**Muijres, F. T., Elzinga, M. J., Iwasaki, N. A. and Dickinson, M. H.** (2015). Body saccades of *Drosophila* consist of stereotyped banked turns. *Journal of Experimental Biology* **218**, 864–875.

**Mureli, S. and Fox, J. L.** (2015). Haltere mechanosensory influence on tethered flight behavior in *Drosophila*. *Journal of Experimental Biology* 2528–2537.

**Mureli, S., Thanigaivelan, I., Schaffer, M. L. and Fox, J. L.** (2017). Cross-modal influence of mechanosensory input on gaze responses to visual motion in *Drosophila*. *Journal of Experimental Biology* **220**, 2218–2227.

**Nalbach, G.** (1993). The halteres of the blowfly *Calliphora*. *Journal of Comparative Physiology A* **173**, 293–300.

**Namiki, S., Dickinson, M. H., Wong, A. M., Korff, W. and Card, G. M.** (2018). The functional organization of descending sensory-motor pathways in drosophila. *Elife* **7**, e34272.

**Namiki, S., Ros, I. G., Morrow, C., Rowell, W. J., Card, G. M., Korff, W. and Dickinson, M. H.** (2022). A population of descending neurons that regulates the flight motor of *Drosophila*. *Current Biology* **32**, 1–8.

**Noah, J. A., Quimby, L., Frazier, S. F. and Zill, S. N.** (2004). Walking on a “peg leg”: Extensor muscle activities and sensory feedback after distal leg denervation in cockroaches. *J Comp Physiol A Neuroethol Sens Neural Behav Physiol* **190**, 217–231.

**Pringle, J. W. S.** (1948). The gyroscopic mechanism of the halteres of Diptera. *Philosophical Transactions of the Royal Society B: Biological Sciences* **233**, 347–384.

**Rauscher, M. J. and Fox, J. L.** (2020). Weighted haltere and imposed haltere stroke reduction tethered flying *Drosophila* kinematics. *Dryad, Dataset*.

**Rauscher, M. J. and Fox, J. L.** (2021). Haltere and visual sensory inputs sum linearly to predict wing (but not head) motor output in tethered flying *Drosophila*. *Proceedings of the Royal Society B* **288**, 20202374.

**Reiser, M. B. and Dickinson, M. H.** (2008). A modular display system for insect behavioral neuroscience. *J Neurosci Methods* **167**, 127–139.

**Sherman, A. and Dickinson, M. H.** (2003). A comparison of visual and haltere-mediated equilibrium reflexes in the fruit fly *Drosophila melanogaster*. *Journal of Experimental Biology* **206**, 295–302.

**Sherman, A. and Dickinson, M. H.** (2004). Summation of visual and mechanosensory feedback in *Drosophila* flight control. *Journal of Experimental Biology* **207**, 133–142.

**Strausfeld, N. J. and Seyan, H. S.** (1985). Convergence of visual, haltere, and prosternal inputs at neck motor neurons of *Calliphora erythrocephala*. *Cell Tissue Res* **240**, 601–615.

**Sun, M., Wang, J., Xiong, Y., Sun, M., Wang, J. and Xiong, Y.** (2007). Dynamic flight stability of hovering insects. *Acta Mech Sin* **23**, 231–246.

**Suver, M. P., Huda, A., Iwasaki, N., Safarik, S. and Dickinson, M. H.** (2016). An array of descending visual interneurons encoding self-motion in *Drosophila*. *The Journal of Neuroscience* **36**, 11768–11780.

**Trimarchi, J. R. and Murphey, R. K.** (1997). The shaking-B2 mutation disrupts electrical synapses in a flight circuit in adult *Drosophila*. *Journal of Neuroscience* **17**, 4700–4710.

**Tu, M. S. and Dickinson, M. H.** (1996). The control of wing kinematics by two steering muscles of the blowfly (*Calliphora vicina*). *Journal of Comparative Physiology A 1996 178:6* **178**, 813–830.

**Wannier, T., Bastiaanse, C., Colombo, G. and Dietz, V.** (2001). Arm to leg coordination in humans during walking, creeping and swimming activities. *Experimental Brain Research 2001 141:3* **141**, 375–379.

**Wiggin, T. D., Peck, J. H. and Masino, M. A.** (2014). Coordination of fictive motor activity in the larval zebrafish is generated by non-segmental mechanisms. *PLoS One* **9**, e109117.

**Yarger, A. M. and Fox, J. L.** (2018). Single mechanosensory neurons encode lateral displacements using precise spike timing and thresholds. *Proceedings of the Royal Society B: Biological Sciences* **285**, 20181759.

**Zill, S. N. and Moran, D. T.** (1981). The exoskeleton and insect proprioception. I. Responses of tibial campaniform sensilla to external and muscle-generated forces in the American cockroach, *Periplaneta americana*. *Journal of Experimental Biology* **91**, 1–24.

**Figure 1. Electromagnetic control of haltere movement asynchronous from the wings.**
**(A)** Schematic of iron filing treatment (top, inset) and electromagnetic stimulation system (bottom). **(B)** Representative traces showing movement of untreated haltere at wingbeat frequency (~200Hz), immobilized haltere treated with iron filing (ii), and actively-driven haltere at a range of frequencies controlled by electromagnets (iii-viii) **(C)** Haltere tracking by condition, registered into a normalized body coordinate system defining the haltere base as the origin, represented by circle and the anterior wing base as (0,1), represented by asterisk. Colors reflect the z-normalized wingstroke elevation at each measurement point. **(D)** Mean FFT (95% confidence interval shaded) of all high-speed (1000 or 2000fps) time series with the haltere immobilized (black), driven at 36Hz (blue), and 72Hz (teal). **(E)** same as (D) for 25Hz (red) and 50Hz (pink) frequencies. **(F)** same as (D) and (E) for 100Hz (orange) and 167Hz (magenta) frequencies. **(G-I)** Haltere stroke amplitude (G), peak angular velocity (H) and baseline wingbeat frequencies (I) observed under each haltere manipulation. Lines show median for each group. 167Hz responses from outlier animal shown with +. Letters denote statistical groupings from multiple Bonferroni-corrected Wilcoxon rank-sum test (5% alpha).

**Figure 2. Haltere manipulation increases saccade rate in kinematic outputs downstream of halteres.** **(A).** Schematic of measured kinematic outputs, recorded at 100fps, showing downstroke amplitude (angle of wing envelope leading edge) for each wing and yaw movement of the head. (B) Example ipsilateral wing amplitude traces under haltere treatment conditions. Positive-going angles denote counterclockwise changes in the projected wing envelope leading edge angle which for the right-hand wing (as in all depicted examples) signifies an increase in downstroke amplitude. **(C)** Ipsilateral wing saccade rates from all haltere treatments (see Methods). Left and right wing responses for symmetrical manipulations (untreated, bilateral ablation) are pooled. Lines show median for each group. Letters denote statistical groupings from multiple Bonferroni-corrected Wilcoxon rank-sum test (5% alpha). **(D,E)** Same as (C) for contralateral wing and head saccade rates, respectively. **(F)** Saccade-triggered average ipsilateral wing amplitude responses for each condition (Shade, 95% confidence interval). Gray triangles showed the saccade peak, around which each constitutive video segment of the STA is indexed. **(G)** Same as (F) but for the baseline-subtracted instantaneous wingbreat frequency.

**Figure 3 Ipsilateral wing saccades are more likely when the haltere exceeds normal kinematic parameters**
**(A)** Summary of haltere angular position, angular velocity, and wing instantaneous phase from all high speed data, separated by condition. (Ai) Untreated animals, showing natural antiphase synchrony of haltere and wings. Inset shows unified body coordinate scheme, with haltere upstrokes typically occupying the 45-90° range and downstrokes typically occupying the 235-270° range (Aii) Frames from haltere immobilized (magnets OFF) condition. Green dashed line shows extent of the naturalistic parameter space observed in the untreated animal. (Aiii) High-speed frames aggregated from all magnetic stimulation frequencies, showing broad overlap with the naturalistic range of haltere angular velocities and angular positions. **(B)** Histograms of ipsilateral wing amplitude video frames showing probability of saccade as a function of haltere angular position at frame onset for each condition. **(C).** Same as (B) but for haltere signed-RMS angular velocity throughout the frame (see Methods). Light green shaded regions outline the naturalistic range of negative (upstroke) and positive (downstroke) angular velocities. **(D)**. Same as (B) but for wing instantaneous phase at frame onset.

**Figure 4. Haltere manipulation increases broadband noise in kinematic outputs downstream of halteres.** **(A)** Example ipsilateral wing amplitude traces under haltere treatment conditions, as in Fig.2A-B **(B)** FFT of traces from (A), showing peaks at the frequency of the actively-driven example at 36Hz and increases in broadband noise of both actively and passively manipulated halteres as compared to the untreated example. Dashed line shows fold frequency for kinematics camera framerate **(C)** Area under curve (AUC) measurements for FFTs from all haltere treatments (see Methods). Left and right wing responses for symmetrical manipulations (untreated, bilateral ablation) are pooled. Lines show median for each group. Letters denote statistical groupings from multiple Bonferroni-corrected Wilcoxon rank-sum test (5% alpha). **(D,E)** Same as (C) for contralateral wing and head AUCs, respectively.

**Figure 5. Haltere manipulations influence visually-guided wing and head movements.**
**(A)** Schematic of visual stimulus, showing irregular stripe pattern moving on an LED panel under the control of a 1Hz triangle-wave with a pattern velocity of 90°/s **(B)** Example ipsilateral wing amplitude responses to visual stimulus under several haltere treatment conditions. **(C)** FFTs of traces from (B), showing peak at the frequency of the visual stimulus. **(D)** Ipsilateral wing response amplitude at visual stimulus frequency for all tested haltere treatments. For symmetrical manipulations (untreated, bilateral ablation), left and right wing responses are pooled. Letters denote statistical groupings from multiple Bonferroni-corrected Wilcoxon rank-sum test (5% alpha). **(E,F)** Same as (D) for contralateral wing and head yaw responses, respectively. Lines show median for each group. **(G)** Ipsilateral wing visual response magnitude, as estimated by measuring FFT magnitude at visual stimulus frequency, for untreated flies, haltere-immobilized flies, and 36Hz magnetic stimulation flies. Trendlines connect median data from each pattern velocity, with shaded region showing 1$^{st}$ and 3$^{rd}$ quartiles. Inset, results of Kruskal-Wallis omnibus test indicate whether pattern velocity is a significant predictor of response amplitude within each treatment group (*) or not (ns). **(H-I)** Same as (G), but for contralateral wing and head yaw amplitude, respectively.

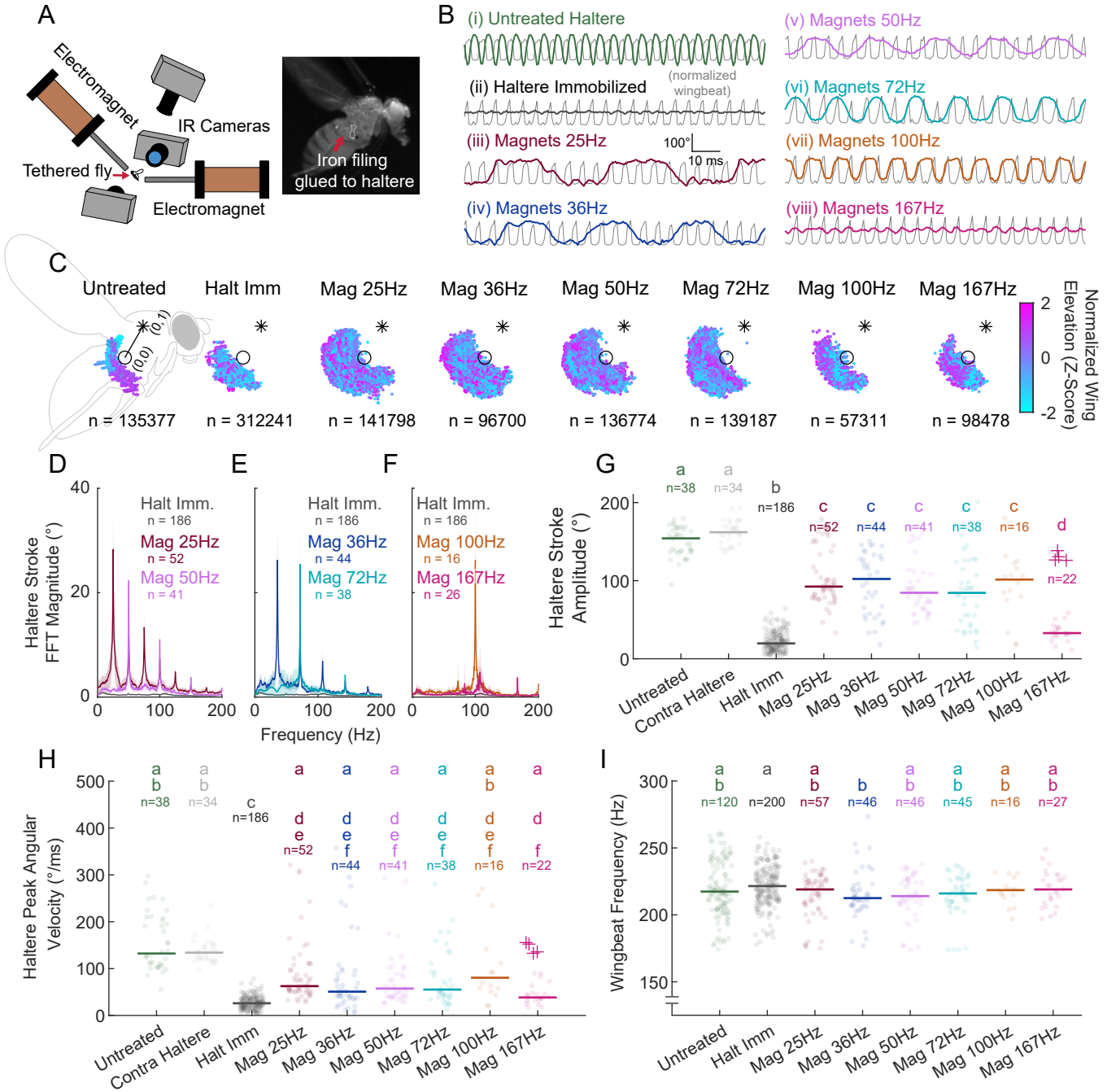
A
Electromagnet
IR Cameras
Tethered fly
Electromagnet
Iron filing glued to haltere
B
(i) Untreated Haltere
(ii) Haltere Immobilized
(normalized wingbeat)
(iii) Magnets 25Hz
100°
10 ms
(iv) Magnets 36Hz
(v) Magnets 50Hz
(vi) Magnets 72Hz
(vii) Magnets 100Hz
(viii) Magnets 167Hz
C
Untreated
Halt Imm
Mag 25Hz
Mag 36Hz
Mag 50Hz
Mag 72Hz
Mag 100Hz
Mag 167Hz
(0,1)
(0,0)
n = 135377
n = 312241
n = 141798
n = 96700
n = 136774
n = 139187
n = 57311
n = 98478
Normalized Wing Elevation (Z-Score)
2
0
-2
D
E
F
Haltere Stroke FFT Magnitude (°)
Halt Imm.
n = 186
Mag 25Hz
n = 52
Mag 50Hz
n = 41
Mag 36Hz
n = 44
Mag 72Hz
n = 38
Mag 100Hz
n = 16
Mag 167Hz
n = 26
Frequency (Hz)
G
Haltere Stroke Amplitude (°)
Untreated
Contra Haltere
Halt Imm
Mag 25Hz
Mag 36Hz
Mag 50Hz
Mag 72Hz
Mag 100Hz
Mag 167Hz
H
Haltere Peak Angular Velocity (°/ms)
I
Wingbeat Frequency (Hz)

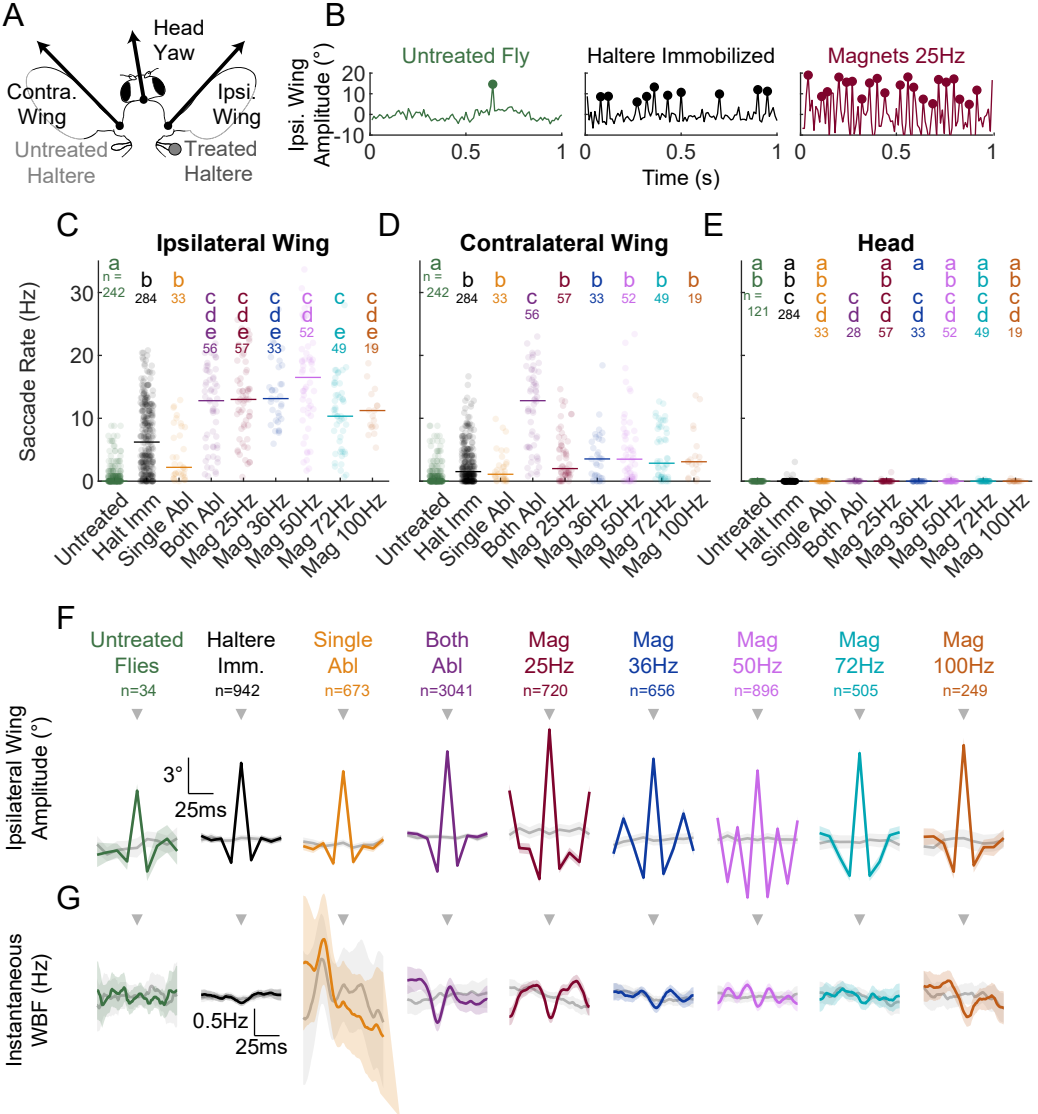
A
Head Yaw
Contra. Wing
Ipsi. Wing
Untreated Haltere
Treated Haltere
B
Untreated Fly
Haltere Immobilized
Magnets 25Hz
Ipsi. Wing Amplitude (°)
Time (s)
C
Ipsilateral Wing
D
Contralateral Wing
E
Head
Saccade Rate (Hz)
Untreated
Halt Imm
Single Abl
Both Abl
Mag 25Hz
Mag 36Hz
Mag 50Hz
Mag 72Hz
Mag 100Hz
F
Untreated Flies n=34
Haltere Imm. n=942
Single Abl n=673
Both Abl n=3041
Mag 25Hz n=720
Mag 36Hz n=656
Mag 50Hz n=896
Mag 72Hz n=505
Mag 100Hz n=249
Ipsilateral Wing Amplitude (°)
3°
25ms
G
Instantaneous WBF (Hz)
0.5Hz
25ms

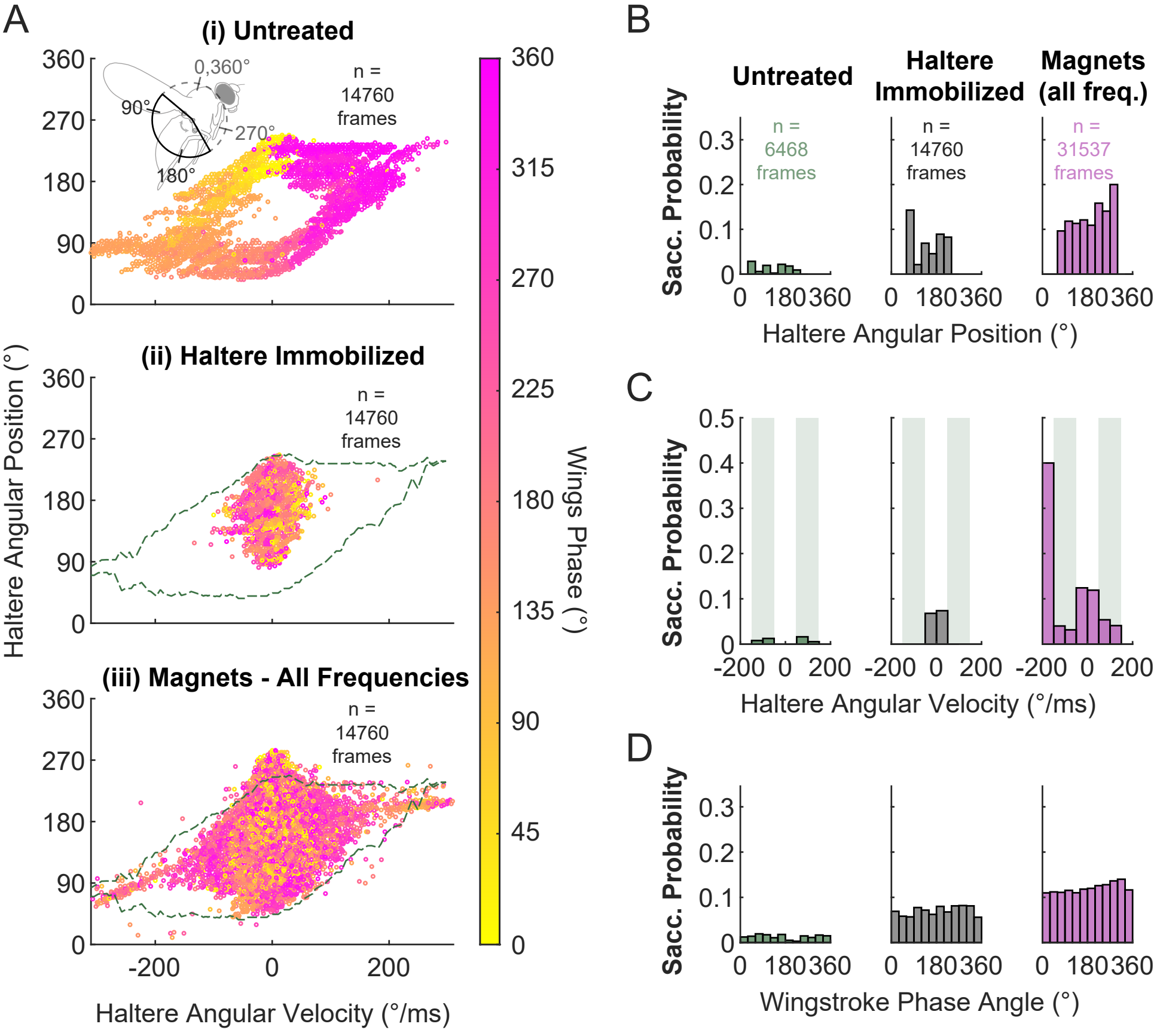
A
(i) Untreated
0,360°
90°
270°
180°
n = 14760 frames
(ii) Haltere Immobilized
n = 14760 frames
(iii) Magnets - All Frequencies
n = 14760 frames
Haltere Angular Position (°)
Haltere Angular Velocity (°/ms)
Wings Phase (°)
B
Untreated
Haltere Immobilized
Magnets (all freq.)
n = 6468 frames
n = 14760 frames
n = 31537 frames
Sacc. Probability
Haltere Angular Position (°)
C
Sacc. Probability
Haltere Angular Velocity (°/ms)
D
Sacc. Probability
Wingstroke Phase Angle (°)

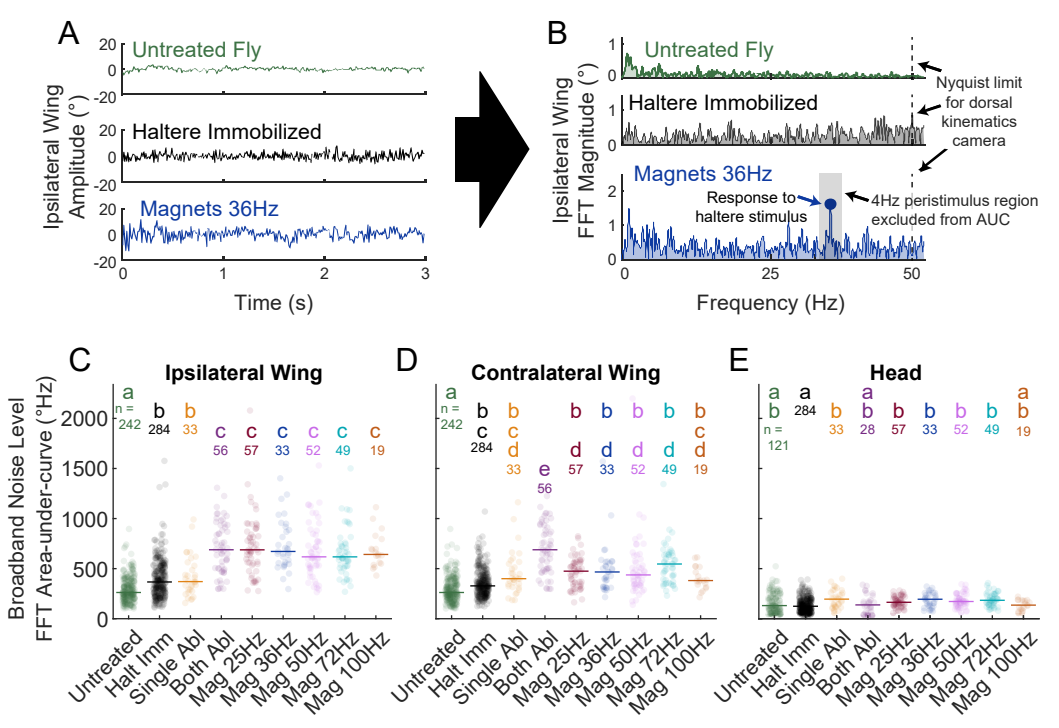
A
Untreated Fly
Haltere Immobilized
Magnets 36Hz
Ipsilateral Wing Amplitude (°)
Time (s)
B
Untreated Fly
Haltere Immobilized
Magnets 36Hz
Ipsilateral Wing FFT Magnitude (°)
Nyquist limit for dorsal kinematics camera
Response to haltere stimulus
4Hz peristimulus region excluded from AUC
Frequency (Hz)
C
Ipsilateral Wing
D
Contralateral Wing
E
Head
Broadband Noise Level FFT Area-under-curve (°Hz)
Untreated
Halt Imm
Single Abl
Both Abl
Mag 25Hz
Mag 36Hz
Mag 50Hz
Mag 72Hz
Mag 100Hz

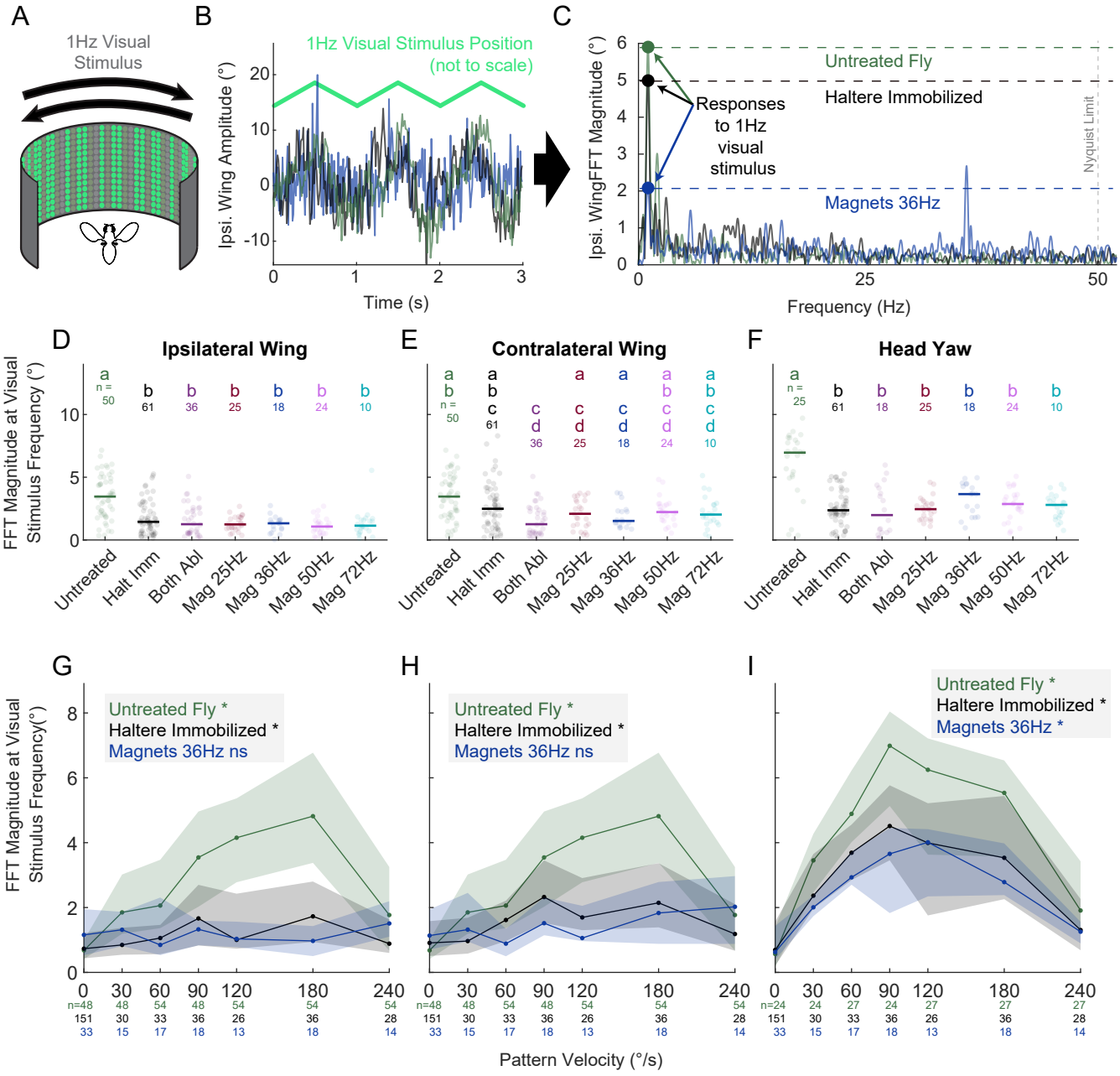
A
1Hz Visual Stimulus
B
1Hz Visual Stimulus Position (not to scale)
Ipsi. Wing Amplitude (°)
Time (s)
C
Untreated Fly
Haltere Immobilized
Responses to 1Hz visual stimulus
Magnets 36Hz
Nyquist Limit
Ipsi. WingFFT Magnitude (°)
Frequency (Hz)
D
Ipsilateral Wing
E
Contralateral Wing
F
Head Yaw
FFT Magnitude at Visual Stimulus Frequency (°)
Untreated
Halt Imm
Both Abl
Mag 25Hz
Mag 36Hz
Mag 50Hz
Mag 72Hz
G
H
I
Untreated Fly *
Haltere Immobilized *
Magnets 36Hz ns
Magnets 36Hz *
Pattern Velocity (°/s)